

1 **BIM reconstruction from 3D point clouds: A semantic registration approach based on**
2 **multimodal optimization and architectural design knowledge**

3 Fan Xue, Weisheng Lu, Ke Chen, Chris Webster
4

This is the peer-reviewed post-print version of the paper:

Xue, F., Lu, W., Chen, K., & Webster, C. J. (2019). BIM reconstruction from 3D point clouds: A semantic registration approach based on multimodal optimization and architectural design knowledge. *Advanced Engineering Informatics*, 42, 100965.

Doi: [10.1016/j.aei.2019.100965](https://doi.org/10.1016/j.aei.2019.100965)

The final version of this paper is available at: <https://doi.org/10.1016/j.aei.2019.100965>.

The use of this file must follow the [Creative Commons Attribution Non-Commercial No Derivatives License](https://creativecommons.org/licenses/by-nc-nd/4.0/), as required by [Elsevier's policy](https://www.elsevier.com/locate/elsevierpolicy).

5
6 **Abstract**

7 Reconstructing semantically rich building information model (BIM) from 2D images or 3D
8 point clouds represents a research realm that is gaining increasing popularity in architecture,
9 engineering, and construction. Researchers have found that architectural design knowledge,
10 such as symmetry, planarity, parallelism, and orthogonality, can be utilized to improve the
11 effectiveness of such BIM reconstruction. Following this line of enquiry, this paper aims to
12 develop a novel semantic registration approach for complicated scenes with repetitive,
13 irregular-shaped objects. The approach first formulates the architectural repetition as the
14 multimodality in mathematics. Thus, the reconstruction of repetitive objects becomes a
15 multimodal optimization (MMO) problem of registering BIM components which have accurate
16 geometries and rich semantics. Then, the topological information about repetition and
17 symmetry in the reconstructed BIM is recognized and regularized for BIM semantic
18 enrichment. A university lecture hall case, consisting of 1.9 million noisy points of 293 chairs,
19 was selected for an experiment to validate the proposed approach. Experimental results showed
20 that a BIM was satisfactorily created (achieving about 90% precision and recall) automatically
21 in 926.6s; and an even more satisfactory BIM achieved 99.3% precision and 98.0% recall with
22 detected semantic and topological information under the minimal effort of human intervention
23 in 228.4s. The multimodality model of repetitive objects, the repetition detection and
24 regularization for BIM, and satisfactory reconstruction results in the presented approach can
25 contribute to methodologies and practices in multiple disciplines related to BIM and smart city.
26

27 **Keywords**

28 Building information model, architectural repetition, multimodal optimization, semantic
29 enrichment, 3D point cloud
30

31 **1 Introduction**

32 The research reported in this paper is positioned in a small but rapidly growing body of
33 literature on reconstruction of building information models (BIM) (Tang et al. 2010; Valero et
34 al. 2016; Belsky et al. 2016; Xue et al. 2018). A BIM is a digital representation of physical and
35 functional characteristics of a facility to enhance data interoperability and information sharing
36 in the building lifecycle (NIBS 2015). The keyword in the term ‘BIM’ is ‘information’ (Lu et
37 al. 2019). Schlueter & Thesseling (2009) classified BIM information into three categories
38 including geometric, semantic and topological, whereby geometric information directly relates
39 to the building form in three dimensions; semantic information describes the properties of
40 components (i.e., more advanced rule and function information); and topological information
41 captures the dependencies of components. Semantics will become more important as BIM
42 grows into a mature technology in architecture, engineering, construction, and even smart city
43 development.

44
45 Not many existing built facilities have a semantically rich BIM. One approach to make up such
46 fault is to enrich a BIM’s semantics manually. The manual method, albeit accurate, is tedious
47 and time-consuming (Chen et al. 2015). The cost of manual semantics enrichment may far
48 exceed the values that the enriched BIM semantics can generate. Therefore, researchers in
49 recent years have endeavored to deploy various semi-automatic or automatic methods to
50 reconstruct BIM from high-quality yet inexpensive measurement data, e.g., satellite images, or
51 3D point clouds, and enrich semantics in the BIM (Huber et al. 2011; Xiong et al. 2013;
52 Barazzetti 2016; Jung et al. 2016; Thomson & Boehm 2015; Pătrăucean et al. 2015).

53
54 Volk et al. (2014) categorizes the BIM reconstruction methods into two subclasses, i.e., “data-
55 driven” and “model-driven,” based on their principles; while another well-known taxonomy
56 distinguishes “Scan-vs-BIM” from “Scan-to-BIM” regarding the involvement of as-designed
57 BIM in inputs (Bosché, et al. 2013). However, most approaches in the literature of each
58 subclass relied on a generic computer vision process called ‘semantic segmentation’, whereby
59 every point in a 3D point cloud (or a pixel in a 2D image) is assigned to a semantic label first.
60 The semantic segmentation has its fair share of shortcomings which can be largely alleviated
61 by an emerging segmentation-free paradigm (Andreopoulos & Tsotsos 2013; Xue et al. 2019b).
62 For example, the ‘semantic registration’ approach fits semantically rich components into an
63 intermediate BIM by maximizing the similarity (or minimizing the errors) between the
64 reconstructed BIM and the whole measurement data, and subsequently registering them with
65 detected semantic information and topological information (Xue et al. 2019b).

66
67 Along with the considerable progress in developing methods for BIM reconstruction and
68 semantics enrichment, some researchers (e.g. Chen et al. 2018; Wang et al. 2018)
69 serendipitously discovered that architectural design knowledge can be utilized to improve the
70 efficiency and effectiveness of these methods. Architectural features such as symmetries,

71 planarity, parallelism, and orthogonality in relationships between building components,
72 contain rich semantics in their own right. Properly retrieved, they can be rich semantics to be
73 reconstructed into the building information models. Such architectural features are not
74 accidental. Rather, they are the result of functions, economics, mechanics, manufacturing, and
75 aesthetics (Mitra 2008; 2012) and they therefore represent clues in matching geometric pattern
76 with meaning and the related symbolism of language. They can also be applied as constraints
77 to effectively eliminate noise in measurement data and to reduce the search space of formulated
78 problem (Chen et al. 2017).

79
80 Such advances in semantic registration and utilizing architectural domain knowledge have not
81 fully overcome difficulties in dealing with complicated scenes with repetitive, complex-shaped
82 objects. For example, multiple identical furniture measured as identical point cloud patches are
83 the multiple optima, i.e., ‘modes,’ in registering the furniture; but, a unimodal algorithm often
84 wastes computational resources on re-explorations without incorporating efficient search space
85 structures such as the ‘neighborhood’ topology (Du et al. 2015). Thus, the overall efficiency
86 and effectiveness of the existing unimodal registration are relatively low, which is in line with
87 unimodal algorithm’s inferior results on various multimodal benchmark datasets (Chen et al.
88 2010; Li et al. 2013). The multimodal nature triggered us to apply multimodal optimization
89 (MMO) – a well-discussed problem in applied mathematics – to BIM reconstruction in such
90 circumstances.

91
92 In addition, shape and pattern repetition, which conveys important semantics about the design,
93 function, and organization of a facility, has not been widely used for BIM reconstruction. Only
94 a few recent studies have explored the modeling of repetitive structural ribs and piers of a
95 bridge (Hidaka et al. 2018), openings on walls (Dore & Murphy, 2014; Previtali et al. 2018),
96 boundary patterns of rooms (Jung et al. 2018), and indoor furniture (Wang et al. 2018) but they
97 focused on simple-shaped objects or noise-free measurement data. Repetition is actually an
98 ordering principle in architecture leading to sophisticated patterns and structural regularity to
99 support life and well-being in the buildings comprising a city (Ching 2007; Fan et al. 2017).
100 Examples of architectural repetitions exist in furniture setups of conference rooms, patterns or
101 windows on building facades, as well as city blocks. The repetition-based reconstruction for
102 such complex-shaped objects is a research gap that we now address.

103
104 We aim to advance the semantic registration approach for BIM reconstruction by
105 experimenting multimodal optimization algorithms and applying architectural knowledge like
106 repetition patterns. The remainder of the paper is organized as follows. The next section is a
107 literature review covering (a) the paradigmatic change from ‘semantic segmentation’ to
108 ‘semantic registration’ for BIM reconstruction and semantic enrichment; and (b) the
109 opportunities to enhance such semantic registration approaches. The third section is a detailed
110 description of the MMO-based approach in different languages, e.g., mathematical language

111 and pseudocode. The fourth section presents an experiment using a university lecture hall case,
112 consisting of 1.9 million noisy points of 293 chairs as a testbed. Section 5 is an in-depth
113 discussion of the implications and limitations of the research and the last section concludes.

114 115 **2 Literature review**

116 **2.1 From ‘semantic segmentation’ to ‘semantic registration’**

117 In the context of reconstructing BIM from 2D images and 3D point clouds, there are two well-
118 known taxonomies of the BIM reconstruction methods. Volk et al. (2014) categorized the
119 shape-based, shape descriptor-based, and material-based matching methods as “data-driven”
120 methods while knowledge and context-based methods are “model-driven.” Alternatively,
121 Bosché et al. (2013) regarded the BIM reconstruction with referencing to as-designed BIMs as
122 the “Scan-vs-BIM” subclass and those without referential BIM resources as “Scan-to-BIM.”
123 However, most BIM reconstruction applications in the literature, no matter data-driven, model-
124 driven, Scan-to-BIM, or Scan-vs-BIM, relied on semantic segmentation for extracting the
125 object surfaces and creating BIM components (Barazzetti 2016; Babacan et al. 2017).

126
127 Semantic segmentation is a computer vision process that assigns each point (or pixel in 2D
128 images) to a semantic label (Shamir 2008). The segmentation methods involved in BIM
129 reconstruction can be broadly grouped into four types: (i) *a priori* rules, (ii) geometric shape
130 descriptors, (iii) supervised machine learning classifiers, and (iv) a combination of these
131 methods for multiple types of BIM components. The *a priori* rules for BIM component
132 recognition utilize the regularities of individual components, such as the region-growth
133 regarding the planarity of walls and ceilings (Huber et al. 2011) and the prism boundary
134 reconstruction of indoor space (Valero et al. 2012). Explicit shape descriptors extract the
135 characteristic geometric features for shape matching, such as local convexity (Son & Kim 2017)
136 and the Laplace-Beltrami filtering (Wang et al. 2018). Supervised machine learning classifiers
137 such as stacking of logistic regression (Xiong et al. 2013), convolutional neural network
138 (Babacan et al. 2017), and random forest (Bassier, et al. 2019) have also been applied. Many
139 studies employed a combination of multiple segmentation methods for multiple types of BIM
140 components, e.g., Nguyen and Choi (2018) removed planar primitives before the RANSAC
141 fitting of the cylindrical piping systems, and Czerniawski et al. (2018)’s point density-based
142 clustering followed by a bagged decision tree for planar objects. However, these semantic
143 segmentation-based methods have three weaknesses in common: (1) unsatisfactory results for
144 complex-shaped objects (e.g., decorations, furniture, and appliances) (Wang et al. 2018; Zou
145 et al. 2018); (2) reliance on *a priori* rules or labeled data set for training the correlational models;
146 and (3) failure to reuse as-designed or online open BIM resources (Bosché et al. 2013; Xue et
147 al. 2018).

148
149 Segmentation-free methods have thus been developed recently for overcoming these
150 weaknesses. Xue et al. (2018; 2019b) proposed a semantic registration approach that essentially

151 reassembles individual BIM components into a complete model in iterations by minimizing
152 the overall error (or maximizing the similarity) between the reconstructed BIM and the whole
153 measurement data. So far, semantic registration was validated, on both 2D images and 3D point
154 clouds of both indoor and outdoor scenes, e.g., about 80% precision and recall in reconstructing
155 293 theater chairs, using unimodal algorithms such as covariance matrix adaptation evolution
156 strategy (CMA-ES) (Xue et al. 2019b). Hidaka et al. (2018) developed another segmentation-
157 free method, in which similar regions of template CAD models were first adaptively localized
158 then fine-tuned by the iterative closest point (ICP) algorithm. These segmentation-free methods
159 proven to be successful in making use of existing BIM resources (e.g., components collected
160 from open BIM libraries) to enrich the reconstructed BIM with semantics, topology, and fine
161 details.

162

163 However, the segmentation-free methods still suffer from a few limitations (Xue et al. 2019b).
164 The first limitation is that existing segmentation-free methods are not effective and efficient
165 enough for complicated scenes with repetitive, irregular-shaped objects. One of the reasons for
166 this is that existing semantic registration approaches rely on ‘unimodal’ problem solving, in
167 which only one optimal solution can be found in one time. For complicated scenes with
168 repetitive objects, unimodal problem solving suffers the unnecessary re-exploration of the
169 problem search space in the component-by-component processing. The second limitation is the
170 method’s proneness to input errors such as noise, clutters, and occlusion, due to the adoption
171 of the objective functions such as the SSIM (structural similarity), RMSE (root-mean-square
172 error), and the descriptor-based similarity in Hidaka et al. (2018). The last, but not the least,
173 limitation is the availability of online open or as-designed BIM resources and annotated
174 topological requirements, so that they may not work on unique and tailor-made components.

175

176 **2.2 Two opportunities to enhance the ‘semantic registration’ approaches**

177 Multimodal optimization (MMO) can enhance the segmentation-free methods by addressing
178 the first limitation, i.e., to enhance effectiveness and efficiency for complicated scenes. MMO
179 is a class of non-linear optimization that aims to find *all* the optimal solutions (i.e., ‘modes’)
180 to a multimodal problem (Das et al. 2011). For instance, the problem “ $\arg \min_{x \in [0, 10\pi]} \cos(x)$ ”
181 has five solutions, i.e., $1, 3\pi, 5\pi, 7\pi,$ and 9π . Due to the multimodality, an MMO algorithm can
182 find all the five values, while a unimodal algorithm can only find one (Xue et al. 2019b; Kim
183 et al. 2013). MMO algorithms have been applied to many complicated problems with multiple
184 local optima, such as protein structure prediction (Wong et al. 2010) and engineering design
185 (Forrester & Keane 2008). Recent MMO competitions showed that NMMSO (niching
186 migratory multi-swarm optimizer), RS-CMSA-ES (covariance matrix self-adaption evolution
187 strategy with repelling subpopulations), and NEA2+ (niching the CMA-ES via nearest-better
188 clustering) are among the best algorithms (Li et al. 2013; Fieldsend 2014; Ahrari et al. 2017;
189 Qu et al. 2012). For example, NMMSO dynamically manages a large set of Particle Swarm
190 Optimization (PSO) processes for a balanced search for all solutions. MMO algorithms’

191 exclusive capability to handle multimodal problems thus provides an opportunity to
192 complement the existing research of unimodal algorithms for segmentation-free methods for
193 BIM.

194

195 The use of architectural domain knowledge can help address the problem of noisy data and
196 occlusion, i.e., the second limitation of the segmentation-free methods. Several previous
197 studies have made use of architectural domain knowledge in the building reconstruction
198 process. For example, Fisher (2003) described the application of standard feature relations to
199 enhance the building reconstruction. De Luca et al. (2006) proposed a reconstruction approach
200 that used architectural design knowledge to interpret architectural shapes from 3D point clouds.
201 Likewise, Liu and Wu (2016) presented a rule-based method to reconstruct historical building
202 with different architectural styles. In addition, Chen et al. (2018) applied a fundamental
203 regularization rule to rooftop elements from noisy LiDAR point clouds and reconstructed over
204 one thousand buildings located in Hong Kong Island. However, most of these studies were
205 limited by the use only of parallel or orthogonal relationships between building components,
206 paying less attention to the repetitions that embed meaningful architectural domain knowledge.
207 Our anticipation in starting this study was that the two opportunities, i.e., MMO and repetition
208 as architectural domain knowledge, will enhance the ‘semantic registration’ approaches to BIM
209 reconstruction.

210

211 **3 Methodology**

212 To reiterate, this study focuses on developing a novel semantic registration approach to BIM
213 reconstruction by exploring MMO algorithms and making good use of architectural repetition.
214 The approach proposed, as shown in Figure 1, consists of three steps: mathematical formulation,
215 reconstruction of an intermediate BIM based on multimodality of repetition, and regularization
216 of the intermediate BIM using repetition formations. The first two steps are fully automated
217 for an intermediate BIM output based on candidate components with accurate geometry and
218 rich properties, while the last one is semi-automated for the detection and regularization of
219 topological relationships about repetition and symmetry for a final BIM output. There are two
220 differences between the proposed approach and previous semantic registration applications in
221 Xue et al. (2018; 2019b). First, the problem formulation changes from constrained optimization
222 to multimodal optimization, while the solving algorithms which convey automatic
223 reconstruction evolve from unimodal algorithms to MMO ones. Secondly, the architectural
224 design knowledge, such as repetition and symmetry, is applied to recognition and
225 regularization of repetition formations for BIM reconstruction, so that the approach can benefit
226 from both data-driven and model-driven principles.

227

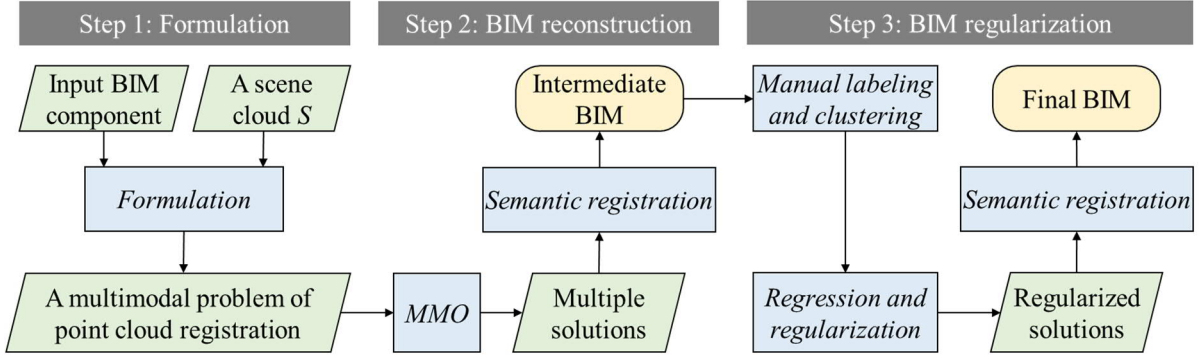


Figure 1. A general framework of the proposed MMO-based semantic registration approach

3.1 Mathematical formulation

The semantic registration approach requires two inputs, i.e., measurement data (e.g., a 3D point cloud or 2D images) and a set of BIM components annotated with topological relationships (Xue, et al. 2019b). To highlight the repetition patterns of components, the BIM reconstruction task in this paper has two data inputs. One input is a ‘scene cloud’ $S = \{p_1, p_2, \dots, p_n\} \subset \mathbb{R}^3$ of n points of repetitive objects. The other is a candidate BIM component of the repetitive objects, such as a parametric Revit family, from which a ‘component cloud’ $\mathcal{C} = \{p_1, p_2, \dots, p_m\} \subset \mathbb{R}^3$ of m visible surface points is evenly sampled. The task of BIM reconstruction is thus equivalent to an optimization problem that finds all the instances of \mathcal{C} in S :

$$\begin{aligned}
 & \mathbf{arg\ min} \quad f(x) = RMSE(\mathcal{C}(x), S) = \left[\frac{1}{m} \sum_{p \in \mathcal{C}(x)} \|p - N(p, S)\|^2 \right]^{1/2} \\
 & \mathbf{s.t.} \quad C(x) \leq 0, \\
 & \quad \mathcal{C}(x) = \{T_x(p) \mid p \in \mathcal{C}\}, \\
 & \quad T_x(p) = \mathbf{R}p + [t_x, t_y, t_z]^T, \\
 & \quad \mathbf{R} = \begin{bmatrix} \cos r_z & -\sin r_z & 0 \\ \sin r_z & \cos r_z & 0 \\ 0 & 0 & 1 \end{bmatrix} \begin{bmatrix} \cos r_y & 0 & \sin r_y \\ 0 & 1 & 0 \\ -\sin r_y & 0 & \cos r_y \end{bmatrix} \begin{bmatrix} 1 & 0 & 0 \\ 0 & \cos r_x & -\sin r_x \\ 0 & \sin r_x & \cos r_x \end{bmatrix}, \\
 & \quad x = [t_x, t_y, t_z, r_x, r_y, r_z]^T \in \mathbb{R}^6
 \end{aligned} \tag{1}$$

where x indicates the six degrees of freedom (DoFs) about 3D translation (i.e., t_x, t_y, t_z) and rotation (i.e., r_x, r_y, r_z), $RMSE$ is the *root-mean-square error* function to minimize, $N(p, S)$ returns the nearest point of p in S , C represents the topological constraints such as “a window must reside on a wall” and “a desk sits on horizontal surfaces” (Belsky et al. 2016; Xue et al. 2018). The expression “ $C(x) \leq 0$ ” is a general form of constraint equations and inequalities, e.g., a constraint $c_1(x) \geq a$ is equivalent to $c_1'(x) = a - c_1(x) \leq 0$, and $c_2(x) = 0$ is equivalent to $c_2(x) \leq 0$ and $c_2'(x) = -c_2(x) \leq 0$. The point cloud $\mathcal{C}(x)$ is a permuted instance of \mathcal{C} transformed by a Euclidean transformation T_x defined on x . \mathbf{R} is a 3×3 orthogonal matrix of rotation, i.e., $\mathbf{R}^T = \mathbf{I}_3$, $[r_x, r_y, r_z]^T$ in x is the (proper) Euler angular vector about the axes, and $t = [t_x, t_y, t_z]^T$ is the translation vector of the origin.

It should be noted that Eq. (1) involves one component for clarity of presentation; it, however, does not degrade the generality of the formulation. The reason lies in the incremental build

253 phase of semantic registration: Given an i -th component and a set $\{ \mathcal{C}_1(x_1), \mathcal{C}_2(x_2), \dots, \mathcal{C}_{i-1}(x_{i-1}) \}$
 254 of $i - 1$ reconstructed components, we can note $\mathcal{C}(x) = \mathcal{C}_i(x) \cup \mathcal{C}_1(x_1) \cup \mathcal{C}_2(x_2) \cup \dots \cup \mathcal{C}_{i-1}(x_{i-1})$
 255 in Eq. (1) to represent the whole model. In the current study, we only uses $RMSE$ in Eq. (1) for
 256 simplicity of the objective function. More as-demanded metrics, such as the *non-*
 257 *correspondence rate* (NCR) (Van Kaick, et al. 2011), values of point colors (grayscale or true
 258 color), and laser reflectance, can extend the f in Eq. (1) in practice.

259

260 An ideal mode (optimal transformation parameters) x^* yields $f(x^*) = f_{\min}$ (e.g., 0), that is,
 261 minimal geometric error (or fully corresponded in case of Eq. (2)) between the permuted
 262 instance cloud $\mathcal{C}(x)$ and the measured scene cloud S . If there are multiple instances of a
 263 parametric BIM component, there should exist multiple modes to Eq. (1). Therefore, it is clear
 264 that the formulated problem is a multimodal problem. However, the point cloud of a real
 265 building or area inevitably has instrumental, environmental, and calibration errors. In addition,
 266 the points of different instances inevitably have heterogeneous point density, geometric
 267 accuracy, occlusion, and clutters. Therefore, the ideal condition of “*arg min*” in Eq. (1) is often
 268 relaxed to a satisfactory condition $f(x^*) \leq \varepsilon$, where ε is a small error tolerance. The set X^* of
 269 multiple satisfactory (Note: rather than ideal or optimal) solutions thus are:

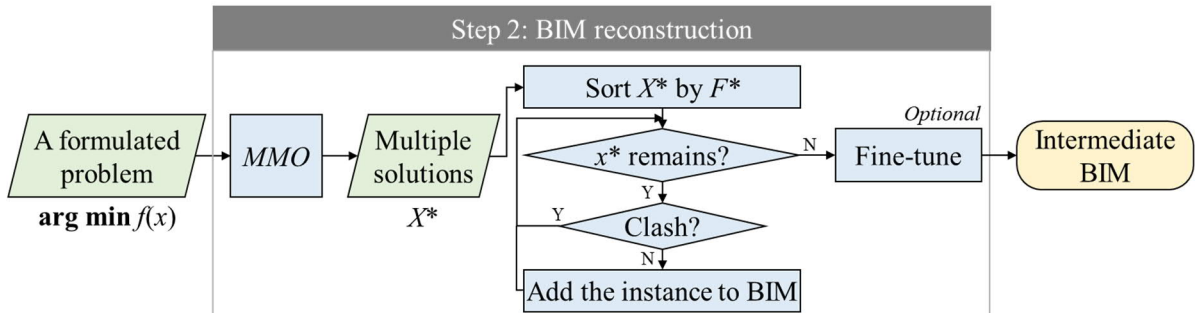
$$X^* = \{ x^* | f(x^*) \leq \varepsilon \}, \quad (3)$$

270 where x^* indicate *one* satisfactory solution (mode) to Eq. (1).

271

272 3.2 BIM reconstruction based on multimodality of repetition

273 The detailed processes of the proposed MMO-based BIM reconstruction is shown in Figure 2.
 274 In general, this step includes the two phases of semantic registration, i.e., the incremental build
 275 phase and the fine-tuning phase. The difference between the proposed approach and Xue et al.
 276 (2019b) is the employment of NMMSO, one of the best MMO algorithms, instead of the
 277 unimodal CMA-ES algorithm due to intrinsic multimodality in the formulated problem. Due
 278 to the evolutionary searching strategies of NMMSO, the unnecessary re-exploration of search
 279 space, a drawback of unimodal semantic registration, was largely eliminated. The proposed
 280 approach was implemented in an in-house developed software plugin COBIMG-Revit
 281 (Constrained Optimization-based Building Information Model Generator-Revit; source code
 282 available at: <https://github.com/ffxue/cobimg>).



283

284 **Figure 2.** Zoom-in of the proposed MMO-based BIM reconstruction for repetitive objects

285

286 As the output of the MMO algorithm, the set X^* in Figure 2 is the multiple satisfactory solutions
287 about the input BIM component, as defined in Eq. (3). However, not every satisfactory solution
288 leads to a feasible instance, this being due to the ε -relaxation which extends the set X^* to include
289 solutions near the optimal solutions. For example, the problem “ $\arg \min_{x \in [0, 10\pi]} \cos(x)$ ” has five
290 exact solutions while the relaxed problem “ $\cos(x) < -1 + \varepsilon, \varepsilon > 0, x \in [0, 10\pi]$ ” has many. MMO
291 algorithms have native strategies, called distance “tolerance”, before forking into new modes,
292 which handles this problem in part. However, the distance tolerance is in 6D in our study,
293 instead of the Euclidean 3D. As a result, there still exist a number of clashes between BIM
294 components if the full set X^* is used for creating new instances.

295

296 A greedy process, as shown in Figure 2, is employed to cleanse the MMO solutions X^* by
297 accepting non-clashed solutions in the reconstruction. First, the objective values F^* of the
298 solutions in X^* are evaluated, so that the set X^* can be sorted in an ascending order of F^* . Then,
299 the solutions in the sorted X^* are tested one by one in order. For each solution, if there is no
300 clash detected between its instance and the BIM comprising of BIM component instances of
301 previous solutions, the new instance is added to the BIM; otherwise, the solution is skipped.
302 After every solution in X^* is tested, the reconstructed BIM is fine-tuned and output as the
303 intermediate BIM. Besides, the object-level semantics, such as materials, production, and usage,
304 is registered to the BIM. It should be noted that the systematic fine-tuning can be omitted in
305 case the MMO algorithm has performed an equivalent processing during its problem solving.
306 After the Step 2, an intermediate BIM is automatically reconstructed with repetitive BIM
307 components.

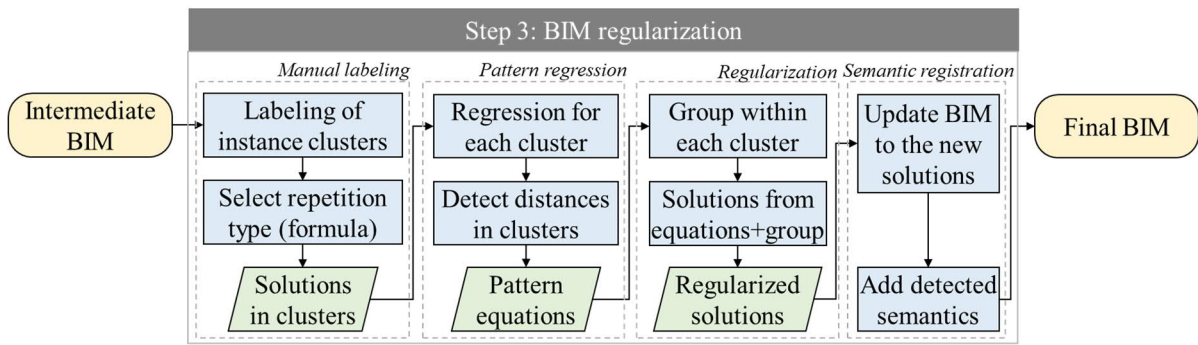
308

309 *3.3 BIM regularization using repetition formations*

310 The intermediate BIM is regularized to create the final BIM. The regularization step aims to
311 correct the errors that come from input data noises or the context-free MMO-based component
312 registration. As shown in Figure 3.a, four modules, i.e., Manual labeling, pattern regression,
313 regularization, and semantic registration, are designed to achieve the aim. In the four modules,
314 only the first one requires human intervention. The regularization was also implemented in our
315 COBIMG-Revit, as shown in Figure 3.b.

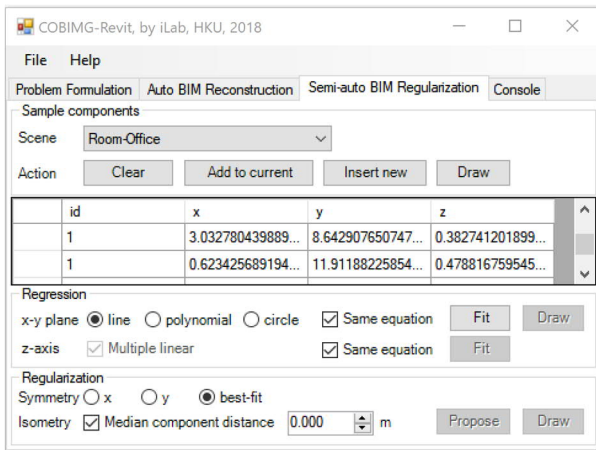
316

317



318

319 (a) Zoom-in of the BIM regularization



320

321 (b) Graphical interface of the COBIMG-Revit plugin

322 **Figure 3.** The BIM regularization process and implementation in an in-house developed
323 software plugin

324

325 In the first module of manual labeling, as shown in Figure 3.a, a human modeler is needed to
326 select a set of components. For example, a row of windows or desks can be quickly labeled as
327 a cluster by dragging a selection box using a mouse and clicking the “Insert new” button in
328 Figure 3.b. In addition, the type of repetition is also chosen by observation of the intermediate
329 BIM. The interim output of the first module is the manually clustered solutions.

330

331 The second module detects the patterns as equations. The pattern equation of each cluster, such
332 as lines or a circle, as well as the uniformed equation of the cross-cluster formation, such as
333 parallel lines and concentric circles, are then regressed for the labeled clusters. COBIMG-Revit
334 realizes the multiple linear regression and the least squares methods for other regression models
335 using two Python scientific libraries *scipy* (version 1.1.0) and *sklearn* (version 0.19.1). The
336 median of nearest distance between components is detected within the clusters.

337

338 The third module proposes new, regularized solutions. Based on the median distance, each
339 cluster can be segmented into smaller groups. The centroids and range of each group are
340 computed from the locations of its members. If an approximate symmetry is detected or defined,
341 two symmetric groups will have perfectly symmetric centroids and ranges. Based on the

342 median distance and the centroid of each group, all the solutions in a cluster can be calibrated
343 isometrically to have a uniform Euclidean distance to their neighbors. In the isometric
344 calibration, new regularized solutions will be proposed along the curve of the pattern equation,
345 while the uniform distance is equal to the median distance. The interim output of this module
346 is the regularized solutions.

347

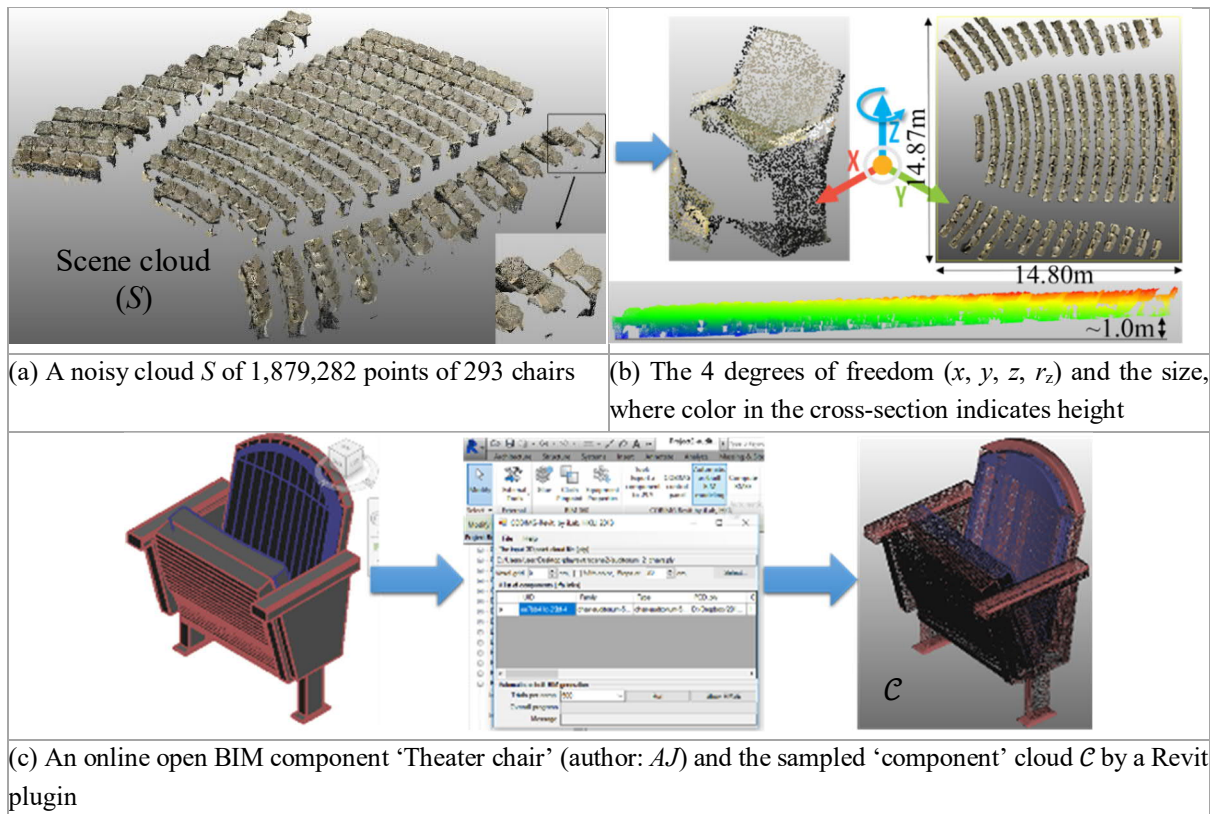
348 The final module revise the intermediate BIM. First, the reconstructed components in BIM are
349 updated using the regularized solutions. Then newly detected topological relationships,
350 including the symmetry, cluster, group, sequence in group, and nearest neighbors, enriches the
351 components to form the final semantically rich BIM. Due to the limited involvement of human
352 intervention, the BIM regularization, as shown in Figure 3, can be regarded as a semi-automatic
353 process.

354

355 **4 Experimental tests**

356 *4.1 Experimental settings*

357 A case of a university lecture hall, which is the “Area_2 Auditorium_2” instance in the Stanford
358 2D-3D-S dataset (Armeni et al. 2017), was selected for validation. The Stanford 2D-3D-S is
359 an open benchmark dataset including a cloud of 695 million annotated indoor points produced
360 from multi-view photos inside a university building (available at
361 <http://buildingparser.stanford.edu/dataset.html>). One reason for targeting an indoor dataset was
362 that it is more challenging in general. The case is also the largest indoor instance in the dataset.
363 The standard exemplar also allows the results of our experiment to be compared with that of a
364 unimodal algorithm CMA-ES in Xue et al. (2019b). To focus on the repetition itself, the
365 semantic labels in the dataset were used to filter 1,879,282 points of 293 theater chairs as the
366 ‘scene’ cloud S , as shown in Figure 4.a, by removing other building elements such as walls and
367 doors which were already annotated in the dataset (Note: For unlabeled indoor scenes, the
368 planarity and normals can segment such elements (Thomson & Boehm 2015)). Some parts of
369 S were noisy, incomplete, and cluttered as shown in Figure 4.a. We assumed that a chair has a
370 possible rotation (heading direction) around the z -axis (Figure 4.b). Thus, there were four
371 degrees of freedoms (DoFs), *i.e.*, the 3D centroid (t_x, t_y, t_z) and the heading direction r_z , for each
372 chair. Ground truth values of the positions of the 293 chairs were extracted from the noisy point
373 cloud and manually validated within an error threshold at 10cm; the true values of heading
374 directions were manually measured with an error threshold at 5° . An online open BIM
375 component ‘Theater chair,’ freely shared by *AJ* at *3DWarehouse.com* (See Figure 4.c), was
376 downloaded for the semantic registration. The input component was selected because it was
377 proven better than some others in Xue et al. (2019b). A ‘component’ cloud C of 1,802,939
378 dense points, as shown in Figure 4.c, was then downsampled from the polygon surface of the
379 volumetric component using an Autodesk Revit (version Educational 64-bit) software plugin
380 developed in Xue et al. (2019b).



381 **Figure 4.** A university lecture hall case and a BIM component using *Autodesk Revit 2015*

382

383 The computational experiments were conducted on a workstation (dual Intel Xeon E5-2690 v4
 384 2.6GHz, 64 GB memory, Windows 10 Enterprise, 56-threading in all tests), with point cloud
 385 library (version 1.8.1) and fast library for approximate nearest neighbor (FLANN, version 1.8.4)
 386 for efficient point cloud processing. The mathematical formation step followed Eq. (3) with
 387 additional settings from Xue et al. (2019b). In the BIM reconstruction step, a C++ version of
 388 the NMMSO algorithm was applied. To make full use of the multi-threading CPUs, the
 389 problem-solving was realized by 110 parallel NMMSO threads, with a maximum of 10,000
 390 iterations. Thus, the maximum number of iterations for BIM reconstruction was equivalently
 391 1.1 million, which is comparable to the 1.4 million ($5,000 \times 289$) iterations of CMA-ES in Xue
 392 et al. (2019b). The swarm size was 300 and the floating-point error tolerance was set to default
 393 (1^{-6}). The results of the NMMSO algorithm automatically registered the template BIM chair to
 394 various positions through the COBIMG-Revit for *Autodesk Revit 2015*. In the BIM
 395 regularization step, the estimated formations of repetition were concentric circles, and the
 396 reflection symmetry and isometry between BIM chairs were also assumed.

397

398 4.2 Experimental results

399 4.2.1 Problem formulation

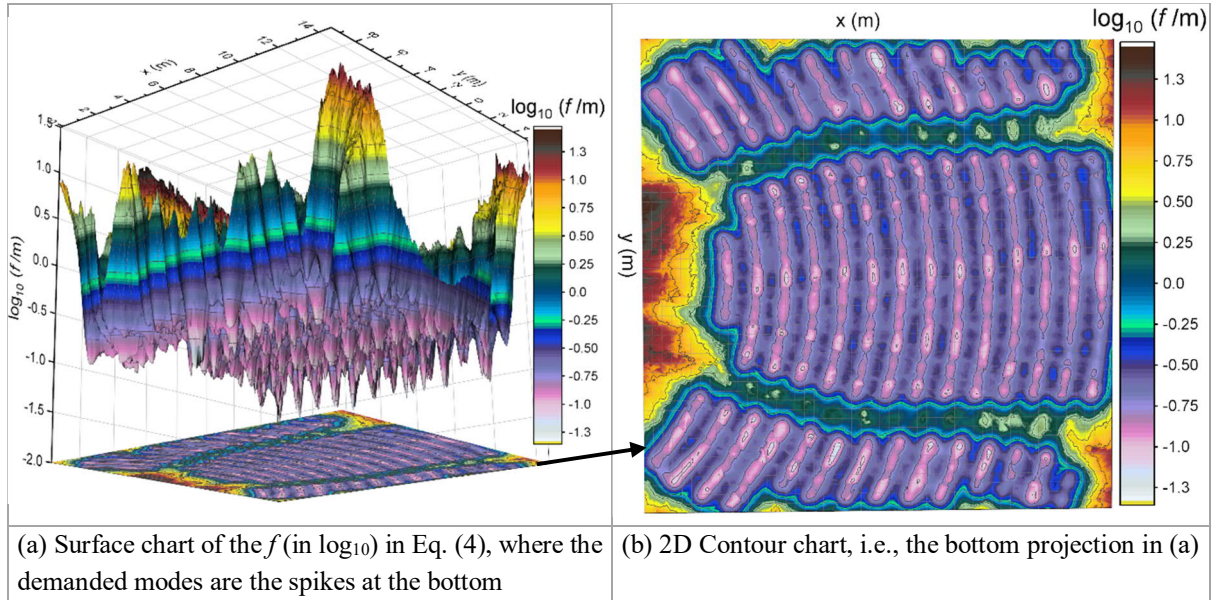
400 Based on Eq. (3), the problem of BIM reconstruction for the university lecture hall was thus:

401

402

$$\begin{aligned}
& \mathbf{arg\ min} \quad f(x) = RMSE(\mathcal{C}(x), S) \\
& \mathbf{s.t.} \quad x = [t_x, t_y, t_z, r_z]^T \\
& \quad \quad parent(\mathcal{C}(x)) = Ground \\
& \quad \quad [t_x, t_y, t_z]^T \in boundingbox(S) \\
& \quad \quad r_z \in [0, 360) \\
& \quad \quad f(x) \leq \varepsilon = 0.25diage \approx 0.01diags
\end{aligned} \tag{4}$$

403 Where *parent* is a function that returns the “parent” component that $\mathcal{C}(x)$ attaches to,
404 *boundingbox* indicates the 3D bounding box of the scene cloud S (see Figure 4.b), *diage* stands
405 for the diagonal length of \mathcal{C} , and *diags* is the diagonal length of the scene cloud S . The tolerance
406 ε is a constant of minimum requirement for a new BIM component, about $1/4\ diage$ and 0.01
407 *diags*, and it can be changed (e.g., to 0.1m or $0.05diage$) for other scenes. Figure 5 visualizes
408 the jagged fitness landscape of Eq. (4) over the x -axis and y -axis. The t_z and r_z in the parameters
409 x were set – after an exhaustive search independent to the experiment – to indicate the best
410 possible f in Figure 5, due to considerably less variance in the z -axis and heading direction than
411 those in the x - y plane. The axes x and y of the spikes in the surface chart, as shown in Figure
412 5.a, are the $[t_x, t_y]^T$ in the demanded modes (optimal transformation parameters); while the best
413 possible f (unit in meter) is shown in logarithm to the base 10 in color to emphasize the modes.
414 It is obvious that there exist many modes for Eq. (4). Figure 5.b shows the contour map, i.e.,
415 the vertical projection, of Figure 5.a. It can be observed from Figure 5b that the modes were
416 highly correlated to the position of the chairs. A very regular formation of the chairs can also
417 be seen, which could be the concentric circles resulting from the architectural acoustic input to
418 the theatre’s design (Mehta et al. 1999).

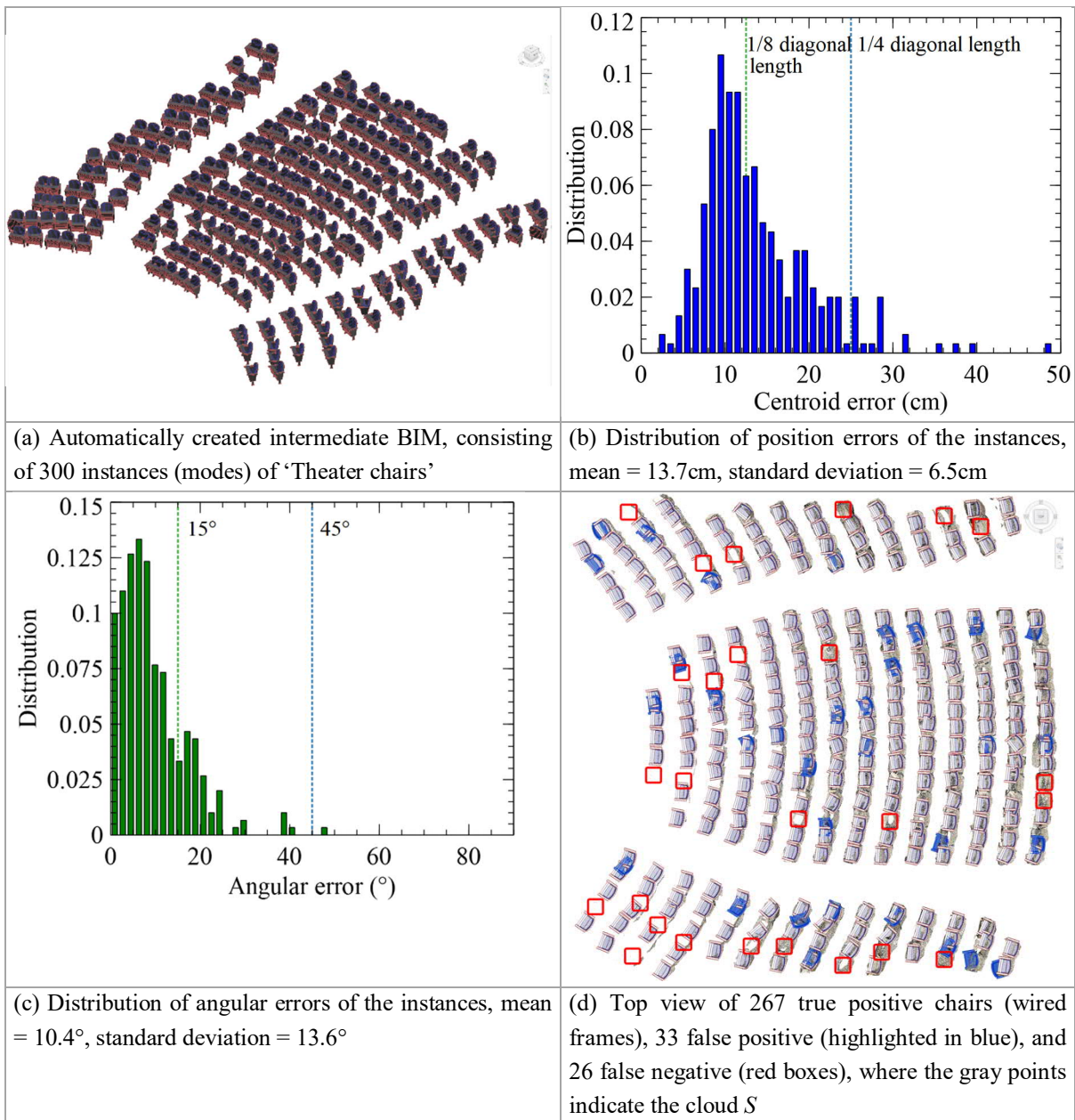


419 **Figure 5.** Visualization of the multimodal fitness landscape of the test case over the x - y plane,
420 where z and r_z were assigned as the best values

421

422 4.2.2 BIM reconstruction

423 The NMMSO algorithm spent 414.5s to find 300 solutions to Eq. (4) in the incremental build
 424 phase using the greedy processing shown in Figure 2. In the second phase of semantic
 425 registration, COBIMG-Revit spent 512.1s on fine-tuning the 300 chairs in BIM using CMA-
 426 ES. The reconstructed intermediate BIM is shown in Figure 6.a. The overall geometry of the
 427 reconstructed BIM looks similar to the input scene, but has some notable gaps with missing
 428 objects. Figure 6.b shows the distribution of centroid errors of the 300 chairs, where the mean
 429 error = 13.7cm, standard deviation = 6.5cm, and about a half of chairs were placed within the
 430 range of 1/8 diagonal length (i.e., the green dashed line of 12.5cm). Figure 6.c visualizes the
 431 distribution of errors of their heading directions, where mean error = 10.4°, standard deviation
 432 = 13.6°, and a considerable portion of chairs were no less than 15° from the referential
 433 directions.



434 **Figure 6.** Intermediate BIM automatically reconstructed in 926.6s by NMMSO

435

436 In order to compare with previous results such as Xue et al. (2019b), the two blue lines were
437 adopted as the acceptance thresholds, i.e., position error $\leq 25\text{cm}$ and angular error $\leq 45^\circ$. In the
438 300 chairs in the reconstructed intermediate BIM, 267 chairs were true positive, 33 were false
439 positive (i.e., wrongly reconstructed). Figure 6.d shows a top view of the chairs in Autodesk
440 Revit, where the false positive are highlighted in blue and 26 false negative (i.e., missing)
441 chairs are in red boxes. Thus,

$$\begin{aligned} \textit{precision} &= \frac{\textit{true positive}}{\textit{true positive} + \textit{false positive}} = 267/300 = 89.0\%, \\ \textit{recall} &= \frac{\textit{true positive}}{\textit{true positive} + \textit{false negative}} = 267/293 = 91.1\%, \\ F_1 &= 2 \times \textit{precision} \times \textit{recall} / (\textit{precision} + \textit{recall}) = 90.1\%. \end{aligned} \quad (5)$$

442 It should be noted that the three metrics may decrease if the acceptance thresholds are changed.

443

444 4.2.3 BIM regularization

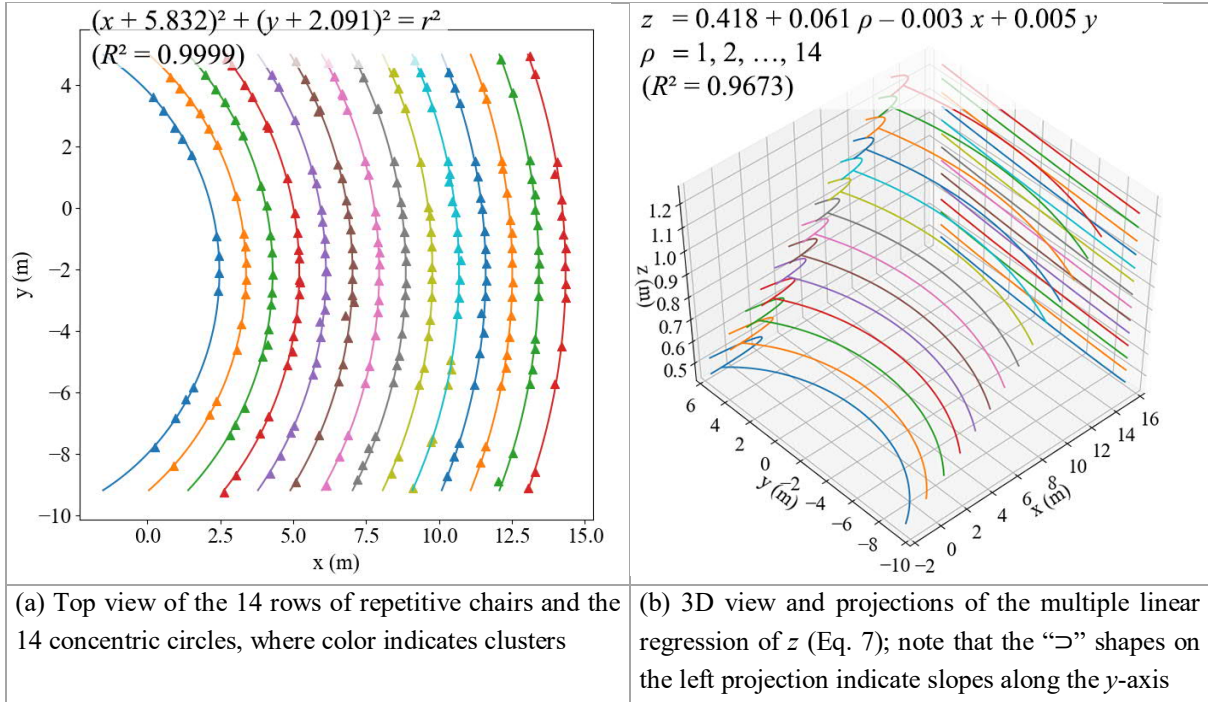
445 Manual labeling grouped the chairs in correct repetition formations as 14 clusters (rows) in
446 223.7 seconds. The centroids of the chairs, as shown in Figure 7.a, were used for the regression.
447 The median distance of two neighboring chairs was 55.26cm. The regression of the equations
448 of the concentric circles (acoustic design patterns) on the x - y plane was conducted using the
449 least square method in 0.06s. The equations obeyed by all chairs were:

$$\begin{aligned} (x + 5.832)^2 + (y + 2.091)^2 &= r^2 && \textit{Concentric circles on the } x\text{-}y \textit{ plane} \\ r &= 0.913 \rho + 7.387 && \textit{with a linear increment on radius} \\ \rho &\in \{1, 2, \dots, 14\} && \textit{The row number from 1 to 14} \\ (R^2 = 0.9999) &&& \textit{A highly satisfactory regression} \end{aligned} \quad (6)$$

450 where the center of the 14 circles, i.e., the stage center, was at $(-5.832, -2.091)$, and the radius
451 r increased linearly against the row number ρ . The equation of z values of the chairs' centroids
452 were further obtained by multiple linear regression against x , y , and ρ using the least squares
453 method in 0.06s:

$$\begin{aligned} z &= 0.418 + 0.061 \rho - 0.003 x + 0.005 y && \textit{A multiple linear regression of } z \\ \rho &\in \{1, 2, \dots, 14\} && \textit{The row number from 1 to 14} \\ (R^2 = 0.9673) &&& \textit{A satisfactory regression} \end{aligned} \quad (7)$$

454 It can be found in Eq. (7) that z had the highest correlation with the row number ρ . In addition,
455 the coefficients $+0.005$ of y and -0.003 of x in Eq. (7) suggested that the repetition formations
456 of chairs had a 1:200 slope over the y -axis and a 1:330 slope over the x -axis, while the $R^2 =$
457 0.9673 confirmed the confidences of the two slopes. As a result, the projections of the 14 curves
458 on the x - z plane were in “ \supset ” shapes. The reason could be that the datum in the Stanford dataset
459 was not perfectly calibrated, or that there were heavy asymmetric errors in the data
460 measurement, or that the lecture hall itself has such an as-designed feature (possibly for
461 drainage) or as-built error.



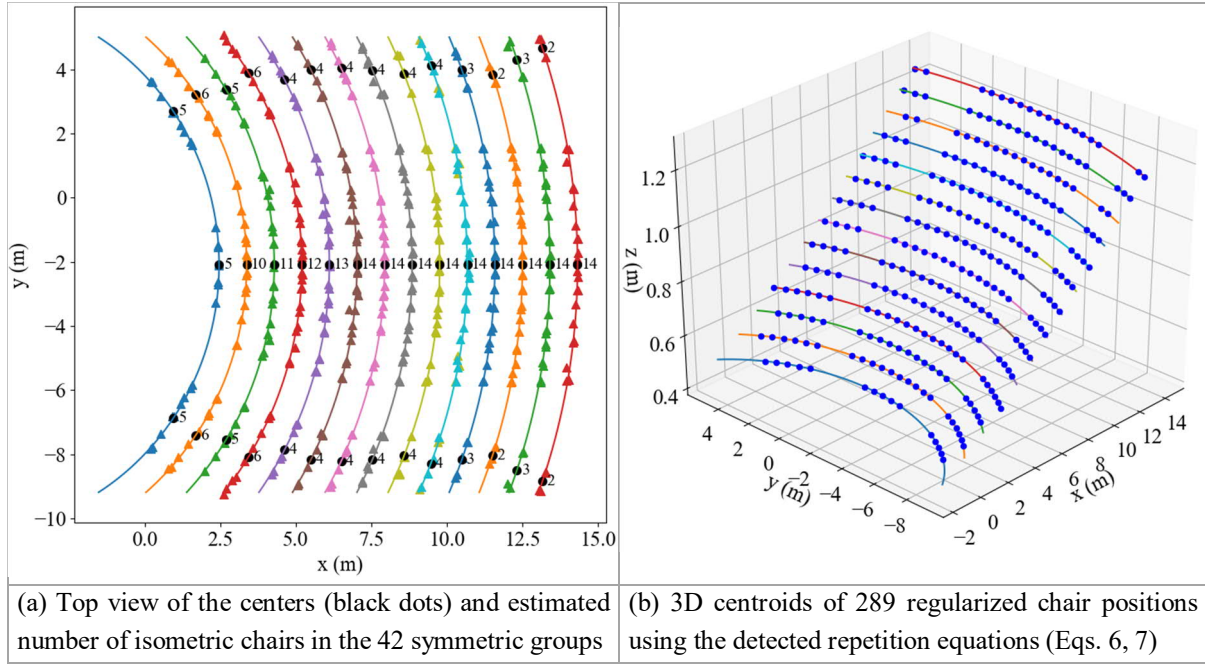
(a) Top view of the 14 rows of repetitive chairs and the 14 concentric circles, where color indicates clusters

(b) 3D view and projections of the multiple linear regression of z (Eq. 7); note that the “D” shapes on the left projection indicate slopes along the y -axis

462 **Figure 7.** Visualization of regression equations of the repetitive BIM components

463

464 Both the symmetric regularization and isometric regularization were set for the BIM chairs.
 465 The symmetric regularization first mirrored all the labeled chairs using the axis $y = -2.091$ (see
 466 Eq. 6) on the x - y plane, and merge the transformed positions to the original ones, as shown in
 467 Figure 8.a. So that most of the missing chairs, i.e., the wrong gaps in the red boxes in Figure
 468 6.b, were filled as shown. In the isometric regularization, the chairs in each extended cluster
 469 were first sorted by a clockwise order of their angles to the center $(-5.832, -2.091)$ and grouped
 470 using a maximum gap (i.e., the minimum aisle width) set at twice the median chair distance (2
 471 $\times 55.26\text{cm}$). Then, the 14 clusters of chairs were split into 42 groups. The center and the
 472 estimated number of isometric chairs in each group are shown in Figure 8.a, where the sum of
 473 the estimated number was 289. Then, 289 new chair positions with isometric distances were
 474 generated on the x - y plane for the 42 groups. The z values were computed by Eq. (7) and the
 475 heading directions were set to the center of the concentric circles, as shown in Figure 8.b.



476 **Figure 8.** Results of the symmetric regularization and isometric regularization based on
 477 repetition in architecture

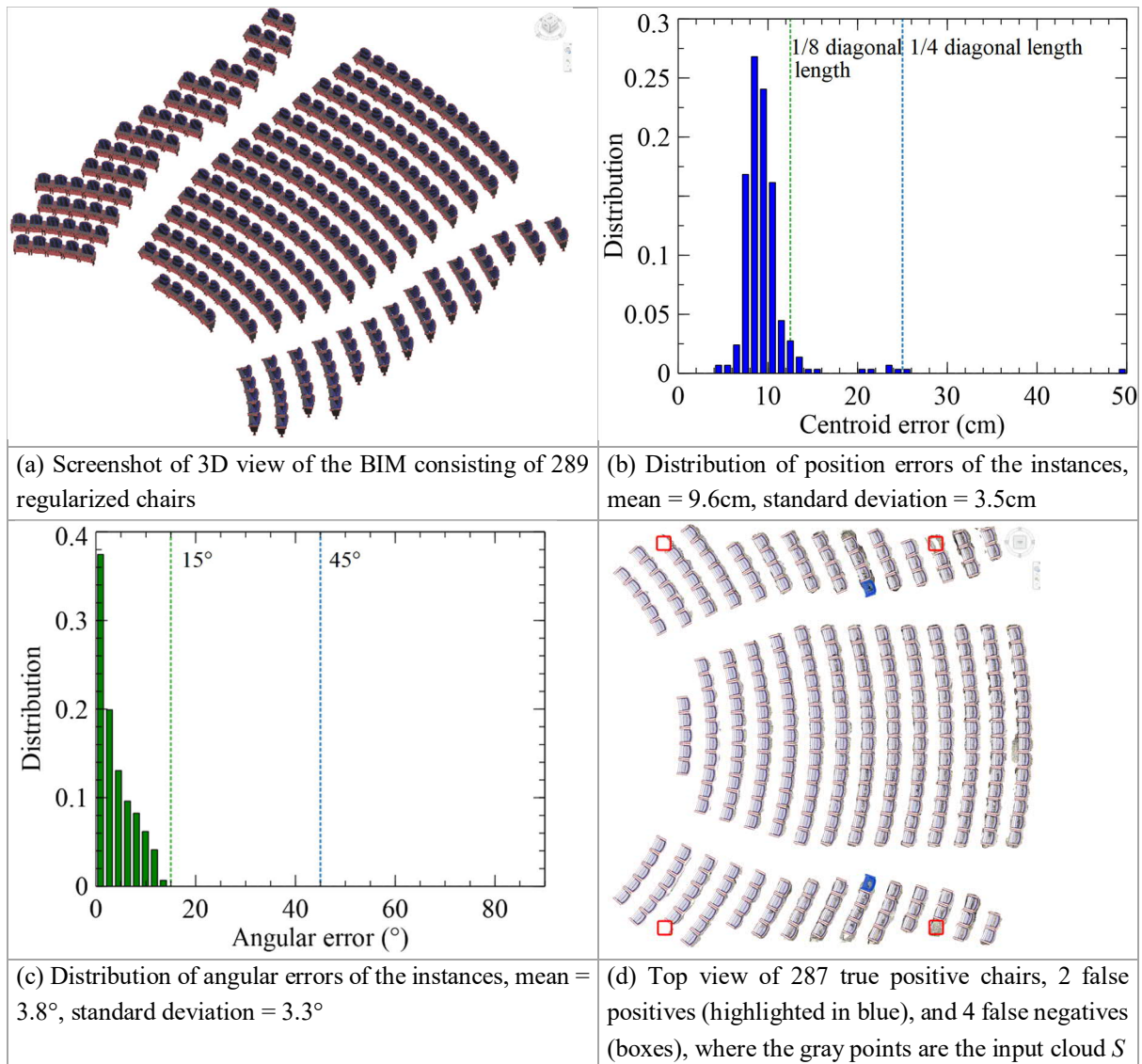
478
 479 The 289 regularized chair positions were used to generate a list of semantics of the regularized
 480 BIM components, as shown in Table 1. Beside the variables involved in Eq. 4, the cluster (row
 481 number), group (theater section), sequence number within group (seat number from right to
 482 left), and neighbors of a BIM component. Examples of neighboring components included the
 483 left, the right, and the one symmetric to the whole plan.

484
 485 **Table 1.** List of semantics and topological relations of the 289 regularized components

Id	Type	Variables in Eq. (4)				Cluster (Row)	Group	Seq. in group	Parent	Neighbors' Ids		
		t_x	t_y	t_z	r_z					Left	Right	Symmetric
1	1	0.255	3.549	0.497	2.318	1	A	1	Ground	2		15
2	1	0.617	3.131	0.493	2.251	1	A	2	Ground	3	1	14
3	1	0.950	2.690	0.490	2.185	1	A	3	Ground	4	2	13
4	1	1.254	2.229	0.487	2.118	1	A	4	Ground	5	3	12
5	1	1.525	1.747	0.484	2.052	1	A	5	Ground		4	11
6	1	2.393	-0.989	0.467	1.704	1	B	1	Ground	7		10
7	1	2.448	-1.539	0.464	1.637	1	B	2	Ground	8	6	9
8	1	2.467	-2.091	0.461	1.571	1	B	3	Ground	9	7	8
9	1	2.448	-2.644	0.458	1.504	1	B	4	Ground	10	8	7
10	1	2.393	-3.193	0.456	1.438	1	B	5	Ground		9	6
11	1	1.525	-5.930	0.444	1.090	1	C	1	Ground	12		5
12	1	1.254	-6.411	0.442	1.023	1	C	2	Ground	13	11	4
13	1	0.950	-6.873	0.440	0.957	1	C	3	Ground	14	12	3
14	1	0.617	-7.314	0.439	0.890	1	C	4	Ground	15	13	2
15	1	0.255	-7.732	0.438	0.824	1	C	5	Ground		14	1
⋮	⋮	⋮	⋮	⋮	⋮	⋮	⋮	⋮	⋮	⋮	⋮	⋮
287	1	14.015	-5.664	1.199	1.393	14	B	14	Ground		286	274
288	1	13.261	-8.582	1.185	1.243	14	C	1	Ground	289		273
289	1	13.076	-9.103	1.183	1.216	14	C	2	Ground		288	272

486

487 The semantics in Table 1 were then registered to form the final BIM as a 1.82 MB Autodesk
 488 Revit project (.rvt) as shown in Figure 9.a, using the COBIMG-Revit plugin in 4.6s. The overall
 489 processing time for the final BIM, including automatic reconstruction and semi-automatic
 490 regularization, was 1,155.0s (i.e., about 3 seconds per chair). The BIM regularization showed
 491 an encouraging improvement as shown in the distributions of position and angular errors in
 492 Figures 9.b and 9.c. As shown in Figure 9.d, the number of true positive chairs increased from
 493 267 to 287, the false positive reduced from 33 to 2, and the false negative reduced from 24 to
 494 4. It is worth noting that none of the 4 missing chairs was detected in the intermediate BIM
 495 before regularization (see Figure 6). As a result, the final BIM had a precision of 99.3%, a
 496 recall of 98.0%, and an F_1 score of 98.6%. The RMSE between the visible surface of the BIM
 497 and the input scene cloud was 8.79cm. In addition, the average distance error and the average
 498 angular error of the final BIM were 9.6cm and 3.8° regarding the ground-truth values,
 499 respectively. Because the majorities in both distributions fall below the two green dashed lines,
 500 the precision and recall rates will remain almost the same if the acceptance thresholds are
 501 tightened to the green dashed lines.

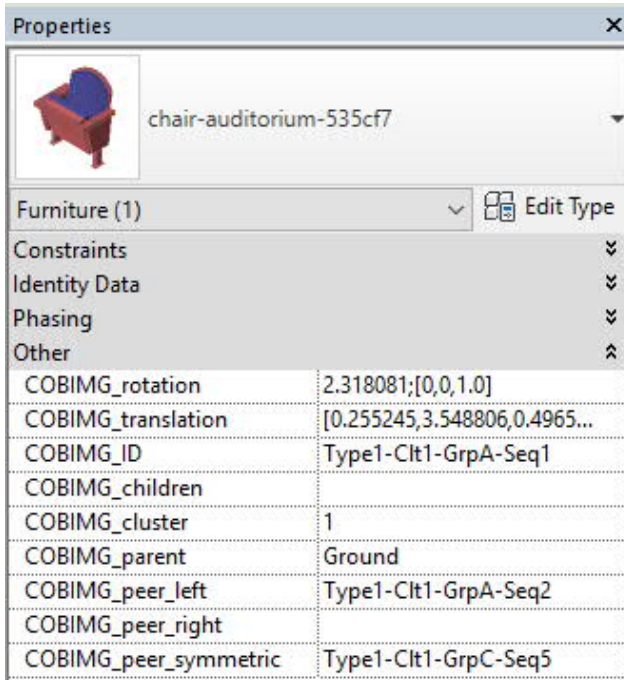


502 **Figure 9.** The final BIM after regularization by the repetition formations

503

504 4.3 Semantics stored in the BIM

505 Rich semantics were also registered to the chairs in the BIM, as a characteristic of the semantic
 506 registration approach. Figure 10 shows the screenshot of the properties of the No. 1 chair listed
 507 in Table 1. The location, heading direction, and parent component, i.e., the invisible “Ground”
 508 was registered as usual. Furthermore, the semantics such as the cluster number, group number,
 509 sequence, and the “neighbor” components were also stored as properties from Table 1.



510

511 **Figure 10.** Screenshot of rich semantics of a chair in the final BIM

512

513 4.4 Comparison to other algorithms

514 The results of the proposed MMO-based approach were compared with two well-known
 515 ‘unimodal’ algorithms ICP (Kim et al. 2013) and CMA-ES (Xue et al. 2019b) applied to the
 516 same test case. Table 2 lists the comparison results, including the RMSE between the input
 517 point cloud and the output BIM, computational time, 3D (t_x , t_y , t_z) position error of chair
 518 centroids, angular error of r_z , precision, recall, and F_1 score, of the BIMs by the four methods
 519 on the pilot case.

520

521

522 **Table 2.** Comparison of different algorithms

<i>Evaluation (unit)</i>	<i>ICP</i> (Kim, et al. 2013)	<i>CMA-ES</i> (Xue, et al. 2019b)	This study	
			Intermediate BIM (automatic)	Final BIM (semi-automatic)
RMSE (cm)	7.28	8.10	10.38	8.97
Computational time (s)	3,702.4	1,434.2	926.6	1,155.0
Number of chair instances	322	288	300	289
Distance error (cm, mean \pm stdev.)	17.9 \pm 10.8	15.2 \pm 7.7	13.7 \pm 6.5	9.6 \pm 3.5
Angular error ($^\circ$, mean \pm stdev.)	28.4 \pm 42.9	17.6 \pm 28.8	10.4 \pm 13.6	3.8 \pm 3.3
Precision (%)	69.3	81.9	89.0	99.3
Recall (%)	76.1	80.5	91.1	98.0
F_1 (%)	72.5	81.2	90.1	98.6

523 (Remark: Bold fonts in each row indicate the best value)

524

525 The first three data columns are the results of three fully automatic methods, i.e., ICP, CMA-
526 ES, and NMMSO (i.e., the intermediate BIM) in this paper. In comparison to unimodal ICP
527 and CMA-ES, the NMMSO outperformed in automatic BIM reconstruction in all aspects
528 except for the RMSE metric defined on points. The precision by NMMSO was about 10%
529 higher than CMA-ES and about 17% higher than ICP, with 35% time saved versus CMA-ES
530 and 75% saved versus ICP. Thus, the pilot study preliminarily confirms the competence of the
531 MMO-based semantic registration approach for automatic BIM reconstruction.

532

533 Furthermore, the effect of using architectural design knowledge can be summarized from the
534 comparison of the last two columns. The Step 3, semi-automatic BIM regularization, resulted
535 in superior results than NMMSO’s intermediate BIM in all aspects except for the time cost.
536 Specifically, the precision (99.3%) and recall (98.0%) became very satisfactory at a
537 computational cost of 228.4s to apply architectural design knowledge. The overall processing
538 time of the proposed approach was 1,155.0s and was less than the two unimodal methods
539 reported in literature.

540

541 **5 Discussion**

542 The experiment reported in this paper confirms the power of a multimodal optimization (MMO)
543 approach to reconstructing semantically rich Building Information Models (BIM). In the
544 methodological sphere, the mathematical concept of multimodality and the practical design
545 rules complement each other to become an efficient (i.e., using less time) and effective (i.e.,
546 more accurate) approach. In the practical sphere, the proposed approach can be easily
547 embedded in mainstream BIM platforms to enable various value-added BIM applications such
548 as architectural design, construction management, heritage conservation, and urban digital twin.

549

550 This study goes beyond existing unimodal ‘semantic registration’ algorithms (e.g., ICP and
551 CMA-ES) and introduces a generic MMO approach so that multiple semantics in measurement

552 data (e.g., 3D point clouds) can be found and registered in a more efficient and effective way.
553 The precision and recall of automatic BIM reconstruction increased from about 80% using
554 unimodal CMA-ES to about 90% using the NMMSO (niching migratory multi-swarm
555 optimizer), and the time cost reduced by about 30%. The experiment further confirms the
556 power of architectural design knowledge (e.g., repetition rules) in improving the efficiency and
557 effectiveness of BIM reconstruction. As-designed or as-built building components need to
558 follow certain rules and the rules can reduce the search space in a formulated BIM
559 reconstruction problem. The repetition rules are utilized as rules for ‘BIM regularization’. After
560 a human-in-the-loop BIM regularization, the precision and recall increased to over 98%, which
561 were close to the ideal values of 100%, while the overall time cost was still less than ICP and
562 CMA-ES.

563

564 Our approach is not weakness free. For example, its scalability needs to be verified in more
565 complicated scenes with different types of repetitive objects. For various scenes, the different
566 sets of repetition formations and algorithm parameter configuration should be comprehensively
567 investigated. In addition, some other limitations of this study should be clarified for future
568 research:

- 569 1. Utilizing architectural domain knowledge for BIM regularization still requires manual
570 intervention for labeling and clustering BIM components. In the reported experiment, the
571 labeling and clustering of chairs cost 223.7 seconds. For more complicated scenes, the
572 increase in the number of different types of repetitive objects will proportionally increase
573 the time needed for manual intervention. In such situations, end-users face a trade-off
574 between accuracy and speed when adopting automatic and semi-automatic approaches to
575 BIM reconstruction. Therefore, how to further automate labeling and clustering is of great
576 importance to further improve the performance of our proposed method.
- 577 2. The method is confirmed to be more robust than existing methods, but false positives and
578 false negatives were still witnessed in the results. In order to further improve accuracy
579 without undue penalty in computation time, additional information and architectural domain
580 knowledge such as the function of the building and local regulations could be used in the
581 BIM reconstruction.
- 582 3. Although the regression and regularization can improve the BIM reconstruction in terms of
583 object recognition and semantics discovery (see Figure 10 and Table 2), the idea of applying
584 the as-designed patterns to a cluster can impose the risk of “regularizing” some as-built
585 errors caused by poor craftsmanship or deformation). In this case, the modeler can simply
586 undo the regularized components back to their as-built status.

587

588 The legitimacy of BIM reconstruction and semantic enrichment needs to be justified in terms
589 of cost-benefit. BIM researchers have developed various reconstruction methods, including
590 ‘semantic segmentation’ and ‘semantic registration’. Our study recognizes the strengths and
591 weaknesses of the semantic registration approach and further improves it by introducing

592 additional algorithms from other disciplines. It demonstrates the power of architectural domain
593 knowledge in improving the effectiveness and efficiency of such approaches. In this sense, the
594 research opens up a new avenue for exploring semantic registration algorithms enhanced by
595 architectural design knowledge.

596

597 **6 Conclusion**

598 This study advances the realm of semantically rich BIM reconstruction by addressing the
599 widespread challenge of dealing with complicated scenes (e.g., indoor environments with
600 repetitive, irregular-shaped objects, and noisy measurement data as input). An MMO-based
601 semantic registration approach for BIM reconstruction was proposed. The approach consists
602 of three steps: multimodal problem formulation based on repetition in architecture; automatic
603 BIM reconstruction based on MMO; and semi-automatic BIM regularization based on
604 repetition formations. The proposed approach was prototyped and tested in an experiment by
605 following a series of rigorous processes. The experimental results showed that the proposed
606 approach can reconstruct an indoor scene of 293 theater chairs from 1.9 million noisy points
607 with satisfactory accuracy (99.3% precision and 98.0% recall) and less modeling time than
608 previously published algorithms. Our study confirms that the MMO approach, by finding all
609 identical or repetitive objects in one go, is more effective and efficient than traditional
610 ‘unimodal’ problem solving in BIM reconstruction. The research also confirms that
611 architectural domain knowledge, particularly ‘repetition’, can further augment an MMO
612 approach to improve efficiency and effectiveness of BIM reconstruction.

613

614 The paper thus makes significant contributions to the methodology and practice of advanced
615 BIM technologies. An original methodological contribution is to translate the reconstruction
616 of BIM with repetitive objects into a MMO problem, thereby allowing a number of well-
617 established MMO algorithms to be applied to the problem. The paper endorses and extends the
618 paradigmatic shift from ‘semantic segmentation’ to ‘semantic registration’; advances the
619 approach by introducing MMO. Particularly, another novelty of the research is to make use of
620 architectural design knowledge hidden within a point cloud (i.e., symmetry, repetition, and
621 structure regularity), which can be used to eliminate noise or errors of measurement data and
622 to reduce search space of the formulated problem. Augmenting MMO algorithms with
623 architectural domain knowledge is considered a novel philosophy for semantically rich BIM
624 reconstruction. Practically, our approach is suitable for scaling up and embedding in
625 mainstream BIM platforms, for example, to enable value-added applications such as creating
626 BIMs of architectural design, construction management projects, heritage conservation sites
627 and so on, which require accurate mapping of domain-specific semantics to geometric
628 components.

629

630 Future research can be conducted in three directions. First, the effectiveness of the proposed
631 approach should be tested on other complicated cases with less obvious repetitions. Secondly,

632 more advanced computer vision methods can be developed to improve the semi-automatic or
633 manual labeling and clustering deployed in current approach. Thirdly, other types of
634 architectural domain knowledge, including symmetry, architectural styles, historical building
635 materials and technology, local standards and regulations, and parametric curved surfaces, can
636 be tested in BIM reconstruction.

637

638 **Acknowledgements**

639 This study was supported in part by two grants from the Hong Kong Research Grant Council
640 (Nos. 17201717, 17200218) and three grants from The University of Hong Kong (Nos.
641 201711159016, 102009741, 20300083). We wish to express our gratitude to the anonymous
642 reviewers for their constructive comments to improve the quality of the paper.

643

644 **References**

- 645 Ahrari, A., Deb, K. & Preuss, M. (2017). Multimodal optimization by Covariance Matrix Self-
646 Adaptation Evolution Strategy with repelling subpopulations. *Evolutionary*
647 *Computation*, 25(3), 439-471. doi:10.1162/evco_a_00182
- 648 Andreopoulos, A. & Tsotsos, J. K. (2013). 50 years of object recognition: Directions forward.
649 *Computer vision and image understanding*, 117(8), 827-891.
650 doi:10.1016/j.cviu.2013.04.005
- 651 Armeni, I., Sax, A., Zamir, A. R. & Savarese, S. (2017). *Joint 2D-3D-Semantic Data for Indoor*
652 *Scene Understanding*. Stanford, CA, USA: ArXiv e-prints.
- 653 Babacan, K., Chen, L. & Sohn, G. (2017). Semantic segmentation of indoor point clouds using
654 Convolutional Neural Network. *ISPRS Annals of Photogrammetry, Remote Sensing*
655 *and Spatial Information Sciences, IV-4(W4)*, 101-108. doi:10.5194/isprs-annals-IV-4-
656 W4-101-2017
- 657 Barazzetti, L. (2016). Parametric as-built model generation of complex shapes from point
658 clouds. *Advanced Engineering Informatics*, 30(3), 298-311.
659 doi:10.1016/j.aei.2016.03.005
- 660 Bassier, M., Van Genechten, B. & Vergauwen, M. (2019). Classification of sensor independent
661 point cloud data of building objects using random forests. *Journal of Building*
662 *Engineering*, 21, 468-477. doi:10.1016/j.job.2018.04.027
- 663 Belsky, M., Sacks, R. & Brilakis, I. (2016). Semantic enrichment for building information
664 modeling. *Computer-Aided Civil and Infrastructure Engineering*, 31(4), 261-274.
- 665 Bosché, F., Guillemet, A., Turkan, Y., Haas, C. T. & Haas, R. (2013). Tracking the built status
666 of MEP works: Assessing the value of a Scan-vs-BIM system. *Journal of computing in*
667 *civil engineering*, 28(4), 05014004. doi:10.1061/(ASCE)CP.1943-5487.0000343
- 668 Bueno, M., Bosché, F., González-Jorge, H., Martínez-Sánchez, J. & Arias, P. (2018). 4-Plane
669 congruent sets for automatic registration of as-is 3D point clouds with 3D BIM models.
670 *Automation in Construction*, 89, 120-134.
- 671 Chen, K., Lu, W., Peng, Y., Rowlinson, S. & Huang, G. Q. (2015). Bridging BIM and building:
672 From a literature review to an integrated conceptual framework. *International Journal*
673 *of Project Management*, 33(6), 1405-1416. doi:10.1016/j.ijproman.2015.03.006

- 674 Chen, K., Lu, W., Xue, F., Tang, P. & Li, L. H. (2018). Automatic building information model
675 reconstruction in high-density urban areas: Augmenting multi-source data with
676 architectural knowledge. *Automation in Construction*, 93, 22-34.
677 doi:10.1016/j.autcon.2018.05.009
- 678 Chen, M. R., Li, X., Zhang, X. & Lu, Y. Z. (2010). A novel particle swarm optimizer
679 hybridized with extremal optimization. *Applied Soft Computing*, 10(2), 367-373.
680 doi:10.1016/j.asoc.2009.08.014
- 681 Ching, F. D. (2007). *Architecture: Form, Space, and Order* (3rd ed.). John Wiley & Sons.
- 682 Czerniawski, T., Sankaran, B., Nahangi, M., Haas, C. & Leite, F. (2018). 6D DBSCAN-based
683 segmentation of building point clouds for planar object classification. *Automation in
684 Construction*, 88, 44-58. doi:10.1016/j.autcon.2017.12.029
- 685 Das, S., Maity, S., Qu, B. Y. & Suganthan, P. N. (2011). Real-parameter evolutionary
686 multimodal optimization—A survey of the state-of-the-art. *Swarm and Evolutionary
687 Computation*, 1(2), 71-88. doi:10.1016/j.swevo.2011.05.005
- 688 De Luca, L., Véron, P. & Florenzano, M. (2006). Reverse engineering of architectural
689 buildings based on a hybrid modeling approach. *Computers & Graphics*, 30(2), 160-
690 176. doi:10.1016/j.cag.2006.01.020
- 691 Dore, C. & Murphy, M. (2014). Semi-automatic generation of as-built BIM façade geometry
692 from laser and image data. *Journal of Information Technology in Construction*, 19(2),
693 20-46.
- 694 Du, W. B., Gao, Y., Liu, C., Zheng, Z. & Wang, Z. (2015). Adequate is better: particle swarm
695 optimization with limited-information. *Applied Mathematics and Computation*, 268,
696 832-838. doi:10.1016/j.amc.2015.06.062
- 697 Fan, H., Zipf, A. & Wu, H. (2017). Detecting repetitive structures on building footprints for
698 the purposes of 3D modeling and reconstruction. *International Journal of Digital Earth*,
699 10(8), 785-797.
- 700 Fieldsend, J. E. (2014). Running up those hills: Multi-modal search with the niching migratory
701 multi-swarm optimiser. *Proceedings of 2014 IEEE Congress on Evolutionary
702 Computation* (pp. 2593-2600). IEEE. doi:10.1109/CEC.2014.6900309
- 703 Fisher, R. (2003). Solving architectural modelling problems using knowledge. *Proceedings of
704 the Fourth International Conference on 3-D Digital Imaging and Modeling*. Banff,
705 Alta., Canada: IEEE. doi:10.1109/IM.2003.1240268
- 706 Forrester, A. & Keane, A. (2008). *Engineering design via surrogate modelling: A practical
707 guide*. John Wiley & Sons.
- 708 Hidaka, N., Michikawa, T., Motamedi, A., Yabuki, N. & Fukuda, T. (2018). Polygonization of
709 point clouds of repetitive components in civil infrastructure based on geometric
710 similarities. *Automation in Construction*, 86, 99-117.
711 doi:10.1016/j.autcon.2017.10.014
- 712 Huber, D., Akinci, B., Oliver, A. A., Anil, E., Okorn, B. E. & Xiong, X. (2011). Methods for
713 automatically modeling and representing as-built building information models.
714 *Proceedings of the NSF CMMI Research Innovation Conference*. Retrieved September
715 18, 2018, from https://ri.cmu.edu/pub_files/2011/1/2011-huber-cmmi-nsf-v4.pdf

- 716 Jung, J., Hong, S., Yoon, S., Kim, J. & Heo, J. (2016). Automated 3D wireframe modeling of
717 indoor structures from point clouds using constrained least-squares adjustment for as-
718 built BIM. *Journal of Computing in Civil Engineering*, 30(4), 04015074.
- 719 Jung, J., Stachniss, C., Ju, S. & Heo, J. (2018). Automated 3D volumetric reconstruction of
720 multiple-room building interiors for as-built BIM. *Advanced Engineering Informatics*,
721 38, 811-825. doi:10.1016/j.aei.2018.10.007
- 722 Kim, C., Son, H. & Kim, C. (2013). Automated construction progress measurement using a 4D
723 building information model and 3D data. *Automation in Construction*, 31, 75-82.
724 doi:10.1016/j.autcon.2012.11.041
- 725 Li, X., Engelbrecht, A. & Epitropakis, M. G. (2013). *Benchmark functions for CEC'2013*
726 *special session and competition on niching methods for multimodal function*
727 *optimization*. Melbourne: Evolutionary Computation and Machine Learning Group,
728 RMIT University. Retrieved from [https://titan.csit.rmit.edu.au/~e46507/cec13-](https://titan.csit.rmit.edu.au/~e46507/cec13-niching/competition/cec2013-niching-benchmark-tech-report.pdf)
729 [niching/competition/cec2013-niching-benchmark-tech-report.pdf](https://titan.csit.rmit.edu.au/~e46507/cec13-niching/competition/cec2013-niching-benchmark-tech-report.pdf)
- 730 Liu, J. & Wu, Z. (2016). Rule-based generation of ancient Chinese architecture from the Song
731 Dynasty. *Journal on Computing and Cultural Heritage*, 9(2), Article 7.
732 doi:10.1145/2835495
- 733 Lu, W., Lai, C. C. & Tse, T. (2019). *BIM and Big Data for Construction Cost Management*.
734 Abingdon, Oxon: Routledge.
- 735 Mehta, M., Johnson, J. & Rocafort, J. (1999). *Architectural acoustics: Principles and design*.
736 Englewood Cliffs, NJ United States: Prentice Hall.
- 737 Nguyen, C. H. & Choi, Y. (2018). Comparison of point cloud data and 3D CAD data for on-
738 site dimensional inspection of industrial plant piping systems. *Automation in*
739 *Construction*, 91, 44-52. doi:10.1016/j.autcon.2018.03.008
- 740 NIBS. (2015). *National BIM Standard - United States Version 3*. Retrieved September 24, 2018,
741 from <http://www.nationalbimstandard.org/nbims-us>
- 742 Pătrăucean, V., Armeni, I., Nahangi, M., Yeung, J., Brilakis, I. & Haas, C. (2015). State of
743 research in automatic as-built modelling. *Advanced Engineering Informatics*, 29(2),
744 162-171. doi:10.1016/j.aei.2015.01.001
- 745 Previtali, M., Díaz-Vilariño, L. & Scaioni, M. (2018). Towards automatic reconstruction of
746 indoor scenes from incomplete point clouds: Door and window detection and
747 regularization. *ISPRS TC-4 Mid-term Symposium 2018* (pp. 507-514). ISPRS.
748 doi:10.5194/isprs-archives-XLII-4-507-2018
- 749 Qu, B. Y., Liang, J. J. & Suganthan, P. N. (2012). Niching particle swarm optimization with
750 local search for multi-modal optimization. *Information Sciences*, 197, 131-143.
751 doi:10.1016/j.ins.2012.02.011
- 752 Schlueter, A. & Thesseling, F. (2009). Building information model based energy/exergy
753 performance assessment in early design stages. *Automation in Construction*, 18(2),
754 153-163.
- 755 Shamir, A. (2008). A survey on mesh segmentation techniques. *Computer Graphics Forum*,
756 27(6), 1539-1556. doi:10.1111/j.1467-8659.2007.01103.x
- 757 Son, H. & Kim, C. (2017). Semantic as-built 3D modeling of structural elements of buildings
758 based on local concavity and convexity. *Advanced Engineering Informatics*, 34, 114-
759 124.

- 760 Tang, P., Huber, D., Akinci, B., Lipman, R. & Lytle, A. (2010). Automatic reconstruction of
761 as-built building information models from laser-scanned point clouds: A review of
762 related techniques. *Automation in Construction*, 19(7), 829-843.
763 doi:10.1016/j.autcon.2010.06.007
- 764 Thomson, C. & Boehm, J. (2015). Automatic geometry generation from point clouds for BIM.
765 *Remote Sensing*, 7(9), 11753-11775. doi:10.3390/rs70911753
- 766 Tran, H., Khoshelham, K., Kealy, A. & Díaz-Vilariño, L. (2019). Shape Grammar Approach
767 to 3D Modeling of Indoor Environments Using Point Clouds. *Journal of Computing in*
768 *Civil Engineering*, 33(1), 04018055.
- 769 Valero, E., Adán, A. & Bosché, F. (2016). Semantic 3D reconstruction of furnished interiors
770 using laser scanning and RFID technology. *Journal of Computing in Civil Engineering*,
771 30(4), 04015053.
- 772 Valero, E., Adán, A. & Cerrada, C. (2012). Automatic method for building indoor boundary
773 models from dense point clouds collected by laser scanners. *Sensors*, 12(12), 16099-
774 16115. doi:10.3390/s121216099
- 775 Van Kaick, O., Zhang, H., Hamarneh, G. & Cohen-Or, D. (2011). A survey on shape
776 correspondence. *Computer Graphics Forum*, 30(6), 1681-1707. doi:10.1111/j.1467-
777 8659.2011.01884.x
- 778 Volk, R., Stengel, J. & Schultmann, F. (2014). Building Information Modeling (BIM) for
779 existing buildings—Literature review and future needs. *Automation in construction*, 38,
780 109-127. doi:10.1016/j.autcon.2013.10.023
- 781 Wang, J., Wu, Q., Remil, O., Yi, C., Guo, Y. & Wei, M. (2018). Modeling indoor scenes with
782 repetitions from 3D raw point data. *Computer-Aided Design*, 94, 1-15.
783 doi:10.1016/j.cad.2017.09.001
- 784 Wong, K. C., Leung, K. S. & Wong, M. H. (2010). Protein structure prediction on a lattice
785 model via multimodal optimization techniques. *Proceedings of the 12th annual*
786 *conference on Genetic and evolutionary computation* (pp. 155-162). ACM.
787 doi:10.1145/1830483.1830513
- 788 Xiong, X., Adan, A., Akinci, B. & Huber, D. (2013). Automatic creation of semantically rich
789 3D building models from laser scanner data. *Automation in Construction*, 31, 325-337.
790 doi:10.1016/j.autcon.2012.10.006
- 791 Xue, F., Lu, W. & Chen, K. (2018). Automatic generation of semantically rich as-built building
792 information models using 2D images: A derivative-free optimization approach.
793 *Computer-Aided Civil and Infrastructure Engineering*, 33(11), 926-942.
794 doi:10.1111/mice.12378
- 795 Xue, F., Lu, W., Chen, K. & Zetkovic, A. (2019b). From ‘semantic segmentation’ to ‘semantic
796 registration’: A derivative-free optimization-based approach for automatic generation
797 of semantically rich as-built building information models (BIMs) from 3D point clouds.
798 *Journal of Computing in Civil Engineering*, *Accepted, in press*, 33(4), 04019024.
799 doi:10.1061/(ASCE)CP.1943-5487.0000839
- 800 Xue, F., Lu, W., Webster, C. J. & Chen, K. (2019a). A derivative-free optimization-based
801 approach for detecting architectural symmetries from 3D point clouds. *ISPRS Journal*
802 *of Photogrammetry and Remote Sensing*, 148, 32-40.
803 doi:10.1016/j.isprsjprs.2018.12.005

804 Zou, C., Colburn, A., Shan, Q. & Hoiem, D. (2018). LayoutNet: Reconstructing the 3D room
805 layout from a single RGB image. *2018 IEEE Conference on Computer Vision and*
806 *Pattern Recognition* (pp. 2051-2059). Salt Lake City, USA: IEEE.

807

808